

# DYNAMIC FINITE ELEMENT ANALYSIS OF THREE-DIMENSIONAL SOIL MODELS WITH A TRANSMITTING ELEMENT

HORST WERKLE

*Hochtief AG, Abt. KTI, Bockenheimer Landstr. 24, 6000 Frankfurt/Main 1, W. Germany*

## SUMMARY

A method for the dynamic finite element analysis of a non-axisymmetric soil model with an axisymmetric boundary is presented. In the non-axisymmetric soil domain an arbitrary discretization with three-dimensional isoparametric solid elements is used. At the boundary a transmitting element is arranged. It is based on the semi-analytical element of Waas and Kausel. The transformation of the stiffness matrix of the Waas/Kausel element with cyclic symmetric displacements to general displacement fields is presented. For earthquake excitation the forces acting on the discretized domain are given. The method is illustrated by the dynamic analysis of an embedded box-type building. The distribution and magnitude of significant section forces are discussed.

## INTRODUCTION

The interaction between soil and structure plays an important role in many problems of structural dynamics, namely for massive, stiff structures supported on medium to soft soils. For small strains, soil can often be modelled as a viscoelastic continuum. Analytical solutions of the equations of motion have been derived for special cases, such as for rigid circular and rectangular foundations on a halfspace. For foundations of irregular shape, numerical solutions based on point or line load solutions have been developed. If a complex geometry of the soil model is to be considered, numerical methods, of which the finite element method is the most important, are used. The structure and the soil around the structure may be discretized using finite elements. However, the discretization of the soil requires the existence of a finite domain with boundaries on which stresses or displacements are prescribed. If these boundaries do not exist naturally, so-called transmitting elements with the mechanical properties of the infinite domain are arranged at the boundary of the discretized domain.<sup>1,2</sup>

The simplest type of a transmitting element, given first by Lysmer/Kuhlemeyer, is based on the assumption that pure shear, compression, or Rayleigh waves are impinging on the boundary under a known angle.<sup>3</sup> These elements are of viscous damper type. Since the angles of incidence are generally not known the method is approximate and requires large model sizes.<sup>4</sup> It should be noted, however, that these simple elements are limited neither to frequency domain analysis nor to linear material behaviour in the discretized domain. In some cases substructuring techniques may be useful to reduce the computational effort.<sup>5</sup>

Another transmitting element was recently given by Gupta *et al.*,<sup>6</sup> to represent a halfspace with a hemispherical excavation. Within the excavation the soil is represented by axisymmetric finite elements with cyclic symmetric displacements. The stiffness of the transmitting element is described by continuously distributed frequency-dependent complex Winkler springs. They are obtained by adjusting the approximate model to the analytical solution for the vertical, horizontal, rocking and torsional motion of a rigid circular plate on a halfspace. The validity of this solution for other kinds of excitation and for complex geometries of the discretized soil (resulting in other types of waves impinging at the boundary) is not apparent.

Transmitting elements, which are based on the solution of the pertinent equations of motion and the boundary conditions in the sense of the finite element method, were first developed by Waas for essentially

two-dimensional (plane and axisymmetric) soil models and displacement fields.<sup>7</sup> They can be arranged near the structure and do not require large model sizes. The soil in the element is horizontally layered with a rigid base. Kausel extended this element for axisymmetric structure and soil models with a cyclic symmetric displacement field.<sup>8,9</sup>

Many structures are not axisymmetric and their representation as plane or axisymmetric may be a gross approximation. A three-dimensional discretization of the soil increases the number of degrees-of-freedom (dof's) considerably. If, for example,  $n$  is the number of dof's in one direction, the corresponding number in a two-dimensional model is  $n^2$  and in a three-dimensional model  $n^3$ . Even when using the Lysmer/Kuhlemeyer element the models are very large. Therefore simplified models have been proposed to account approximately for the three-dimensionality of the soil. According to Lysmer *et al.*<sup>10,11</sup> dampers are arranged at the nodes of a plane strain model to absorb shear or Rayleigh waves propagating perpendicular to the plane. It should be noted that the stiffness is evaluated on purely two-dimensional models and that damping may be overestimated by the additionally arranged dampers. It is therefore difficult and not generally possible to assess the accuracy of the results.<sup>12</sup>

Transmitting elements, which are based on a two- or three-dimensional solution of the equations of motion can reduce the required size of the finite element model and the computational effort considerably, compared to approximate elements. Therefore they are especially important for three-dimensional soil models. The purpose of the present study is to extend the range of applicability of the Waas/Kausel transmitting element to cases where the structure or the soil in the discretized domain is not axisymmetric. For this purpose a transformation of the stiffness matrix of the axisymmetric element is presented. The transmitting element obtained represents a layered soil with rigid base and a cylindrical excavation, in which the discretization with three-dimensional solid elements is virtually arbitrary.

### TRANSMITTING ELEMENT

The soil is modelled as a layered viscoelastic medium with a rigid base. The derivation is given in the frequency domain with complex variables to include hysteretic damping. The solution for the stiffness matrix of the axisymmetric transmitting element has been presented for the isotropic medium in detail in Reference 8 and is discussed here briefly.

A general displacement field in the transmitting element can be expanded in a Fourier series as

$$\mathbf{u}_c = \sum_{n=0}^{\infty} (\Phi_n^s \mathbf{u}_n^s + \Phi_n^a \mathbf{u}_n^a) \quad (1)$$

with

$$\mathbf{u}_c = \begin{Bmatrix} u_c \\ w_c \\ v_c \end{Bmatrix} \quad \mathbf{u}_n^s = \begin{Bmatrix} u_n^s \\ w_n^s \\ v_n^s \end{Bmatrix} \quad \mathbf{u}_n^a = \begin{Bmatrix} u_n^a \\ w_n^a \\ v_n^a \end{Bmatrix} \quad (1a)$$

$$\Phi_n^s = \begin{bmatrix} \cos n\varphi & 0 & 0 \\ 0 & \cos n\varphi & 0 \\ 0 & 0 & -\sin n\varphi \end{bmatrix} \quad (1b)$$

$$\Phi_n^a = \begin{bmatrix} \sin n\varphi & 0 & 0 \\ 0 & \sin n\varphi & 0 \\ 0 & 0 & \cos n\varphi \end{bmatrix} \quad (1c)$$

in which  $u_c$ ,  $w_c$  and  $v_c$  are the radial, vertical and tangential displacements, respectively. The superscripts 's' and 'a' refer to symmetry and antisymmetry, respectively, about  $\varphi = 0$ . The inverse relationship for the Fourier coefficients of a general displacement field  $\mathbf{u}_c$  can be written as

$$\mathbf{u}_n^s = \frac{1}{\pi} (1 - \frac{1}{2} \delta_{n0}) \int_0^{2\pi} \Phi_n^s \mathbf{u}_c d\varphi \quad (2a)$$

$$\mathbf{u}_n^a = \frac{1}{\pi} (1 - \frac{1}{2} \delta_{n0}) \int_0^{2\pi} \Phi_n^a \mathbf{u}_c d\varphi \quad (2b)$$

with

$$\begin{aligned} \delta_{n0} &= 0 & \text{for } n \neq 0 \\ &= 1 & \text{for } n = 0 \end{aligned}$$

With this expansion all pertinent equations become uncoupled with respect to  $n$  and to 'a' and 's'. Hence, for the present only 's'-terms for an arbitrary  $n$  will be considered without loss of generality.

The displacements  $\mathbf{u}_n^s$  depend on the radial coordinate  $r$  and the vertical coordinate  $z$ . They can be written as

$$\mathbf{u}_n^s = \mathbf{H}(r) \mathbf{f}(z) \quad (3)$$

where the matrix  $\mathbf{H}(r)$  is that part of the solution of the pertinent equations of motion, which depends upon  $r$ , whereas the functions  $\mathbf{f}(z) = \{f_r(z), f_z(z), f_\varphi(z)\}^T$  are approximated by piecewise linear or quadratic shape functions. For quadratic interpolation the shape functions can be written as

$$\mathbf{f}(z) = \mathbf{N}_\eta \mathbf{f}_0 \quad (4a)$$

$$\mathbf{N}_\eta = [\frac{1}{2}\eta(\eta-1)\mathbf{I}_3, (1-\eta^2)\mathbf{I}_3, \frac{1}{2}\eta(\eta+1)\mathbf{I}_3] \quad (4b)$$

where

$$\mathbf{f}_0 = \{f_r^{l-1}, f_z^{l-1}, f_\varphi^{l-1}, f_r^l, f_z^l, f_\varphi^l, f_r^{l+1}, f_z^{l+1}, f_\varphi^{l+1}\}^T \quad (4c)$$

contains the nodal values of the functions  $\mathbf{f}$  in layer  $l$  and  $\mathbf{I}_3$  is the  $3 \times 3$  unity matrix. The dimensionless local coordinate  $\eta$  corresponds to the global coordinate  $z$  and varies linearly in a single layer from  $-1$  to  $+1$ , Figure 1. The matrix  $\tilde{\mathbf{N}}_\eta$  with the shape functions for linear interpolation is obtained simply by the transformation

$$\tilde{\mathbf{N}}_\eta = \mathbf{\Lambda}^T \mathbf{N}_\eta \mathbf{\Lambda} \quad (5)$$

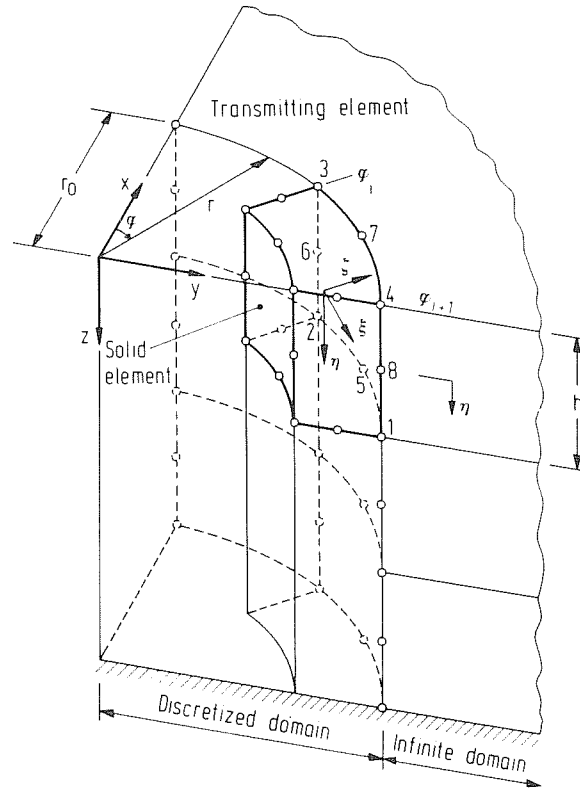


Figure 1. Transmitting element with a single solid element of the discretized domain (one quarter of the complete system)

with

$$\Lambda = \begin{bmatrix} \mathbf{I}_3 & \mathbf{0} \\ \frac{1}{2}\mathbf{I}_3 & \frac{1}{2}\mathbf{I}_3 \\ \mathbf{0} & \mathbf{I}_3 \end{bmatrix} \quad (5a)$$

The dynamic stiffness matrix of the transmitting element can be obtained with the shape functions, equation (3), by a finite element approach. The method is semi-analytic since the shape functions in the horizontal direction fulfill the equations of motion.

Observing homogeneous boundary conditions (zero stress at the soil surface and zero displacements at the base), yields an algebraic eigenvalue problem. The eigenmodes are generalized Rayleigh and Love waves, which propagate or decay exponentially in the layered system, and the eigenvalues are the corresponding wave numbers. The displacements, strains and stresses can be expanded in terms of the eigensolutions. For given displacements at a vertical boundary the corresponding stresses and hence the stiffness matrix of the transmitting element can be determined. One obtains

$$\mathbf{P}_{n,0}^s = \mathbf{R}_n \mathbf{u}_{n,0}^s \quad (6a)$$

$$\mathbf{P}_{n,0}^a = \mathbf{R}_n \mathbf{u}_{n,0}^a \quad (6b)$$

where  $\mathbf{u}_{n,0}^s, \mathbf{u}_{n,0}^a$  contain the Fourier coefficients of the displacements at the layer interfaces at the boundary and  $\mathbf{P}_{n,0}^s, \mathbf{P}_{n,0}^a$  are the corresponding Fourier coefficients of the nodal forces per radian. The stiffness matrix  $\mathbf{R}_n$  for the  $n$ th Fourier coefficient may be used with axisymmetric finite elements in the discretized domain.<sup>8,9</sup>

### NON-AXISYMMETRIC STRUCTURES

In the following the transformation relationships between the axisymmetric and the non-axisymmetric representation of the displacements, forces and the stiffness matrix of the transmitting element are derived. Within the discretized domain, isoparametric solid elements with linear or quadratic shape functions are used.<sup>15</sup> They are well suited to model complex geometries. At the element-boundary interface quadratic shape functions in the tangential direction are used. However, geometrically the quadratic shape of the solid elements does not fit exactly to the circular shape of the transmitting element. The error hereby is small and will be discussed later.

The solid elements are arranged at the boundary, as shown in Figure 1 for a single element. The displacement field along the element side connected with the transmitting element may be written as

$$\mathbf{u}_k = \mathbf{N} \mathbf{u}_e = \mathbf{N}_\eta \mathbf{N}_\xi \mathbf{u}_e \quad (7)$$

$\mathbf{u}_k = \{u_k, v_k, w_k\}^T$  is the vector of the displacements in Cartesian coordinates in  $x, y, z$ -directions, and the vector  $\mathbf{u}_e = \{u_k^{(1)}, v_k^{(1)}, w_k^{(1)}, \dots, w_k^{(8)}\}^T$  contains the corresponding values at the nodal points 1–8 (for linear expansion over  $z$ , points 6 and 8 are omitted). The matrix  $\mathbf{N}$  with the shape functions can be split into  $\mathbf{N}_\eta$ , equation (4a), and  $\mathbf{N}_\xi$ , which depends on the element coordinate  $\xi$ . The element coordinate  $\xi$  corresponds to  $\varphi$  in the global cylindrical coordinate system. For element  $i$  from  $\varphi = \varphi_i$  to  $\varphi = \varphi_{i+1}$  one obtains

$$\xi = a_1 - a_2 \varphi \quad (8)$$

with

$$\begin{aligned} a_1 &= \frac{\varphi_i + \varphi_{i+1}}{\varphi_i - \varphi_{i+1}} \\ a_2 &= \frac{2}{\varphi_i - \varphi_{i+1}} \end{aligned} \quad (8a)$$

Hence the matrix  $\mathbf{N}_\xi$  may be written as

$$\mathbf{N}_\xi = \mathbf{N}_{\xi 0} + \varphi \mathbf{N}_{\xi 1} + \varphi^2 \mathbf{N}_{\xi 2} \quad (9)$$

The matrices  $\mathbf{N}_{\xi 0}, \mathbf{N}_{\xi 1}, \mathbf{N}_{\xi 2}$  are independent on  $\varphi$ . They are defined for quadratic expansion over  $\eta$  as follows:

$$\mathbf{N}_{\xi,j} = \begin{bmatrix} \mathbf{0} & \mathbf{0} & \beta_{3,j} \mathbf{I}_3 & \beta_{2,j} \mathbf{I}_3 & \mathbf{0} & \mathbf{0} & \beta_{5,j} \mathbf{I}_3 & \mathbf{0} \\ \beta_{1,j} \mathbf{I}_3 & \beta_{1,j} \mathbf{I}_3 & \beta_{1,j} \mathbf{I}_3 & \beta_{1,j} \mathbf{I}_3 & \beta_{4,j} \mathbf{I}_3 & \beta_{6,j} \mathbf{I}_3 & \beta_{4,j} \mathbf{I}_3 & \beta_{7,j} \mathbf{I}_3 \\ \beta_{2,j} \mathbf{I}_3 & \beta_{3,j} \mathbf{I}_3 & \mathbf{0} & \mathbf{0} & \beta_{5,j} \mathbf{I}_3 & \mathbf{0} & \mathbf{0} & \mathbf{0} \end{bmatrix} \quad (9a)$$

with  $\beta_{i,j}$ ,  $j = 0, 1, 2$ , according to Table I. (For linear expansion the second row and the sixth and eighth column of the matrix in equation (9a) are omitted.)

Now the element displacement field, equation (7), is transformed into the cylindrical coordinate system by

$$\mathbf{u}_c = \mathbf{T} \mathbf{u}_k \quad (10)$$

with

$$\mathbf{T} = \begin{bmatrix} \cos \varphi & \sin \varphi & 0 \\ 0 & 0 & 1 \\ -\sin \varphi & \cos \varphi & 0 \end{bmatrix} \quad (10a)$$

If this is introduced into equations (2a, b), the result is, for the symmetric Fourier terms,

$$\mathbf{u}_n^s = \frac{1}{\pi} (1 - \frac{1}{2} \delta_{n0}) \mathbf{N}_\eta \sum_{i=1}^m \mathbf{S}_{n,i}^c \mathbf{u}_{c,i} \quad (11a)$$

and, for the antisymmetric terms,

$$\mathbf{u}_n^a = \frac{1}{\pi} (1 - \frac{1}{2} \delta_{n0}) \mathbf{N}_\eta \sum_{i=1}^m \mathbf{A}_{n,i}^c \mathbf{u}_{c,i} \quad (11b)$$

with

$$\mathbf{S}_{n,i}^c = \int_{\varphi_i}^{\varphi_{i+1}} \theta_n^s \mathbf{N}_\xi d\varphi = \int_{\varphi_i}^{\varphi_{i+1}} \theta_n^s d\varphi \mathbf{N}_{\xi 0} + \int_{\varphi_i}^{\varphi_{i+1}} \varphi \theta_n^s d\varphi \mathbf{N}_{\xi 1} + \int_{\varphi_i}^{\varphi_{i+1}} \varphi^2 \theta_n^s d\varphi \mathbf{N}_{\xi 2} \quad (11c)$$

$$\mathbf{A}_{n,i}^c = \int_{\varphi_i}^{\varphi_{i+1}} \theta_n^a \mathbf{N}_\xi d\varphi = \int_{\varphi_i}^{\varphi_{i+1}} \theta_n^a d\varphi \mathbf{N}_{\xi 0} + \int_{\varphi_i}^{\varphi_{i+1}} \varphi \theta_n^a d\varphi \mathbf{N}_{\xi 1} + \int_{\varphi_i}^{\varphi_{i+1}} \varphi^2 \theta_n^a d\varphi \mathbf{N}_{\xi 2} \quad (11d)$$

and

$$\theta_n^s = \begin{bmatrix} \Phi_n^s \mathbf{T} & \mathbf{0} & \mathbf{0} \\ \mathbf{0} & \Phi_n^s \mathbf{T} & \mathbf{0} \\ \mathbf{0} & \mathbf{0} & \Phi_n^s \mathbf{T} \end{bmatrix} \quad (11e)$$

$$\theta_n^a = \begin{bmatrix} \Phi_n^a \mathbf{T} & \mathbf{0} & \mathbf{0} \\ \mathbf{0} & \Phi_n^a \mathbf{T} & \mathbf{0} \\ \mathbf{0} & \mathbf{0} & \Phi_n^a \mathbf{T} \end{bmatrix} \quad (11f)$$

(quadratic expansion for  $\eta$  assumed; for a linear expansion the second 'row' is omitted).

The vector  $\mathbf{u}_{c,i}$  denotes the vector  $\mathbf{u}_c$  for element  $i$ . The analytical solutions of the integrals in equations (11e, f) are given in the appendix. The summation in equations (11a, b) refers to all  $m$  elements in the considered layer and may be understood as assembly of the 'element matrices'  $\mathbf{S}_{n,i}^c$  and  $\mathbf{A}_{n,i}^c$ , respectively.

Table I. Coefficients of the matrix  $\mathbf{N}_{\xi,j}$

	$j = 0$	$j = 1$	$j = 2$
$\beta_{1,j}$	$(a_1^2 - 1)/4$	$-a_1 a_2/2$	$a_2^2/4$
$\beta_{2,j}$	$a_1(a_1 + 1)/2$	$-a_2(1 + 2a_1)/2$	$a_2^2/2$
$\beta_{3,j}$	$a_1(a_1 - 1)/2$	$a_2(1 - 2a_1)/2$	$a_2^2/2$
$\beta_{4,j}$	$(-a_1^2 + 1)/2$	$a_1 a_2$	$-a_2^2/2$
$\beta_{5,j}$	$(-a_1^2 + 1)$	$2a_1 a_2$	$-a_2^2$
$\beta_{6,j}$	$(-a_1 + 1)/2$	$a_2/2$	$0$
$\beta_{7,j}$	$(a_1 + 1)/2$	$-a_2/2$	$0$

The equations (11a, b) may alternatively be written as

$$\mathbf{u}_n^s = \frac{1}{\pi} (1 - \frac{1}{2} \delta_{n0}) \mathbf{N}_\eta \mathbf{S}_n^L \mathbf{u}^L \quad (12a)$$

$$\mathbf{u}_n^a = \frac{1}{\pi} (1 - \frac{1}{2} \delta_{n0}) \mathbf{N}_\eta \mathbf{A}_n^L \mathbf{u}^L \quad (12b)$$

where  $\mathbf{u}^L$  are the nodal point displacements of all solid elements in a single layer and the matrices  $\mathbf{S}_n^L$ ,  $\mathbf{A}_n^L$  are obtained by assembly of the matrices  $\mathbf{S}_{n,i}^e$ ,  $\mathbf{A}_{n,i}^e$ , respectively.

Applying equations (12a, b) to all layers the resulting equations are

$$\mathbf{u}_{n,0}^s = \frac{1}{\pi} (1 - \frac{1}{2} \delta_{n0}) \mathbf{S}_n \mathbf{u}_0 \quad (13a)$$

$$\mathbf{u}_{n,0}^a = \frac{1}{\pi} (1 - \frac{1}{2} \delta_{n0}) \mathbf{A}_n \mathbf{u}_0 \quad (13b)$$

Equations (13a, b) describe the transformation of the vector  $\mathbf{u}_0$  of the nodal displacements at the boundary of the discretized domain into the Fourier coefficients.

Now the transformation of the nodal forces will be considered. This can be obtained by applying the principle of virtual displacements. Equating the virtual work of the point forces  $\mathbf{P}_0$  (corresponding to the displacements  $\mathbf{u}_0$ ) in the discretized domain and the virtual work of the cyclic symmetric forces  $\mathbf{P}_{n,0}^s$ ,  $\mathbf{P}_{n,0}^a$ , one obtains

$$\hat{\mathbf{u}}_0^T \mathbf{P}_0 = \int_0^{2\pi} \sum_{n=0}^{\infty} ((\hat{\mathbf{u}}_n^s)^T (\Phi_n^s)^2 \mathbf{P}_{n,0}^s + (\hat{\mathbf{u}}_n^a)^T (\Phi_n^a)^2 \mathbf{P}_{n,0}^a) d\varphi \quad (14)$$

where the virtual displacements are denoted by  $\hat{\mathbf{u}}$ . If equations (13a, b) are used for the virtual displacements in equation (14) and the indicated integration is performed, one obtains

$$\mathbf{P}_0 = \sum_{n=0}^{\infty} (\mathbf{S}_n^T \mathbf{P}_{n,0}^s + \mathbf{A}_n^T \mathbf{P}_{n,0}^a) \quad (15)$$

All relationships necessary for the transformation of the stiffness matrix are now available. With equations (6a, b, 13a, b, 15) one obtains

$$\mathbf{P}_0 = \mathbf{R} \mathbf{u}_0 \quad (16)$$

The matrix

$$\mathbf{R} = \frac{1}{\pi} \sum_{n=0}^{\infty} (1 - \frac{1}{2} \delta_{n0}) (\mathbf{S}_n^T \mathbf{R}_n \mathbf{S}_n + \mathbf{A}_n^T \mathbf{R}_n \mathbf{A}_n) \quad (17)$$

is the complete stiffness matrix of the transmitting element.  $\mathbf{R}$  is symmetric, since  $\mathbf{R}_n$  is symmetric.

The application of the transformation relationship is not limited to a boundary with cylindrical shape. That is, axisymmetric parts of the discretized domain may be modelled by axisymmetric finite elements and be included in the stiffness matrix  $\mathbf{R}_n$ .

## COMPATIBILITY CONSIDERATIONS

If different types of finite elements are used in the same model, they should be compatible, i.e. there should be no geometric or displacement discontinuity at common edges or surfaces. Both requirements are fulfilled approximately between the transmitting element and the isoparametric solid elements.

Solid elements which are geometrically compatible with the transmitting element require a cylindrical surface at one element side. Although such elements have been derived (see elements SECT9, SECT18, SECT30 in Reference 16) they are not well suited to model complex geometries in the discretized domain. Therefore isoparametric elements have been adopted in the present study. The error implied therewith may be

assessed by considering the greatest gap  $\Delta r$  in the radial direction between the solid element and the transmitting element. Also, the volume  $\Delta V$  'missing' in the integral for the element stiffness matrix may be considered. Figure 2 shows the ratios  $\Delta r/b$  and  $\Delta V/V$ , where  $b$  is the element length and  $V = b \times b \times h$ .<sup>17</sup> They depend on the angle  $\Delta\varphi = \varphi_{i+1} - \varphi_i$  of one solid element or on the number  $m$  of solid elements in one layer. With only eight elements, for example, the ratios  $\Delta r/b \approx 0.1$  per cent and  $\Delta V/V \approx 0.05$  per cent are obtained. With increasing number of elements the error decreases rapidly. It is small compared to other errors involved in a finite element analysis and can therefore be neglected.

The compatibility of the displacement field is given by its representation as a Fourier series, equation (1). However, in numerical analyses only a limited number of Fourier coefficients are considered, so that the compatibility requirement is fulfilled in an approximate sense. The necessary number of Fourier coefficients depends strongly on the actual displacement field at the boundary. As an example the extreme case of a vertical unit displacement of a single nodal point may be considered. The local approximation  $\sigma_n(\varphi)$  of the displacements  $w(\varphi)$  of a solid element with  $\Delta\varphi = \pi/4$  by a Fourier series with 4, 8 and 16 coefficients is shown in Figure 3. The global error in a mean square sense, defined by

$$e = \frac{1}{2\pi} \int_0^{2\pi} (w(\varphi) - \sigma_n(\varphi))^2 d\varphi / w^2(0) \quad (18)$$

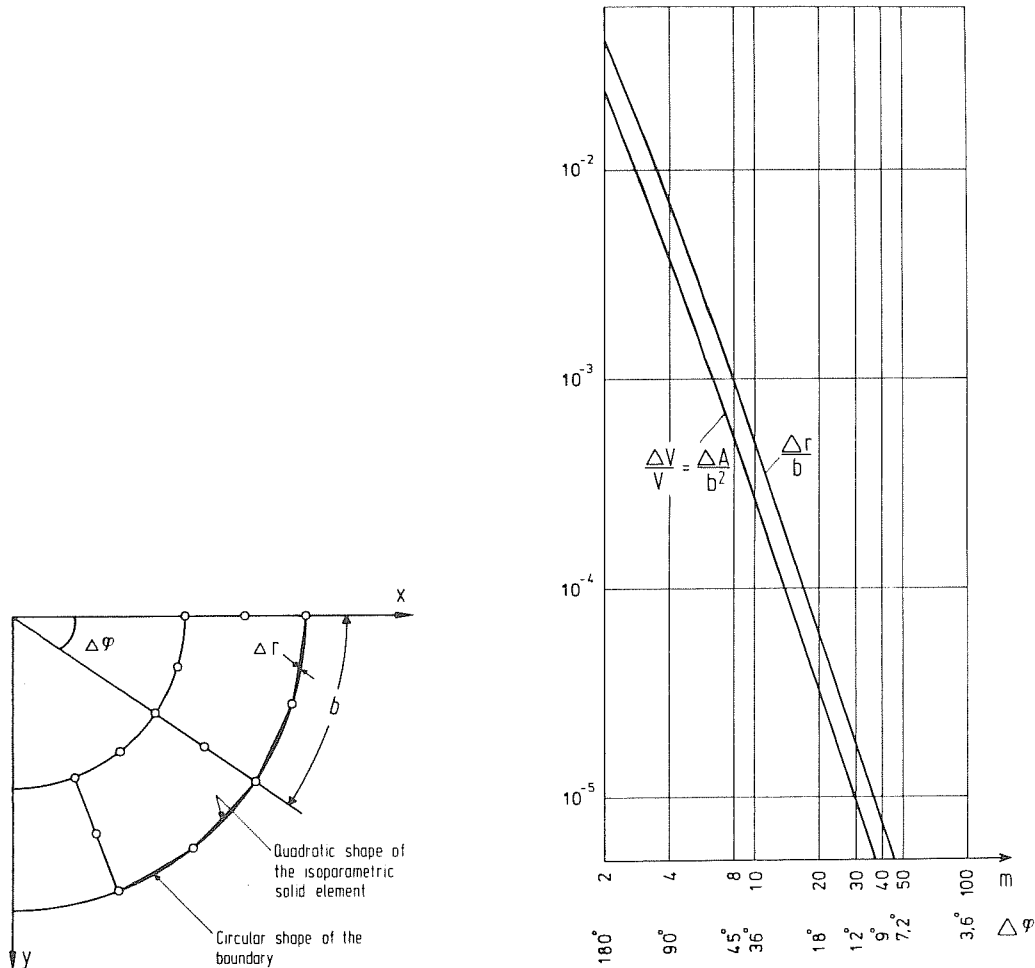


Figure 2. Geometric compatibility of the boundary and the solid elements

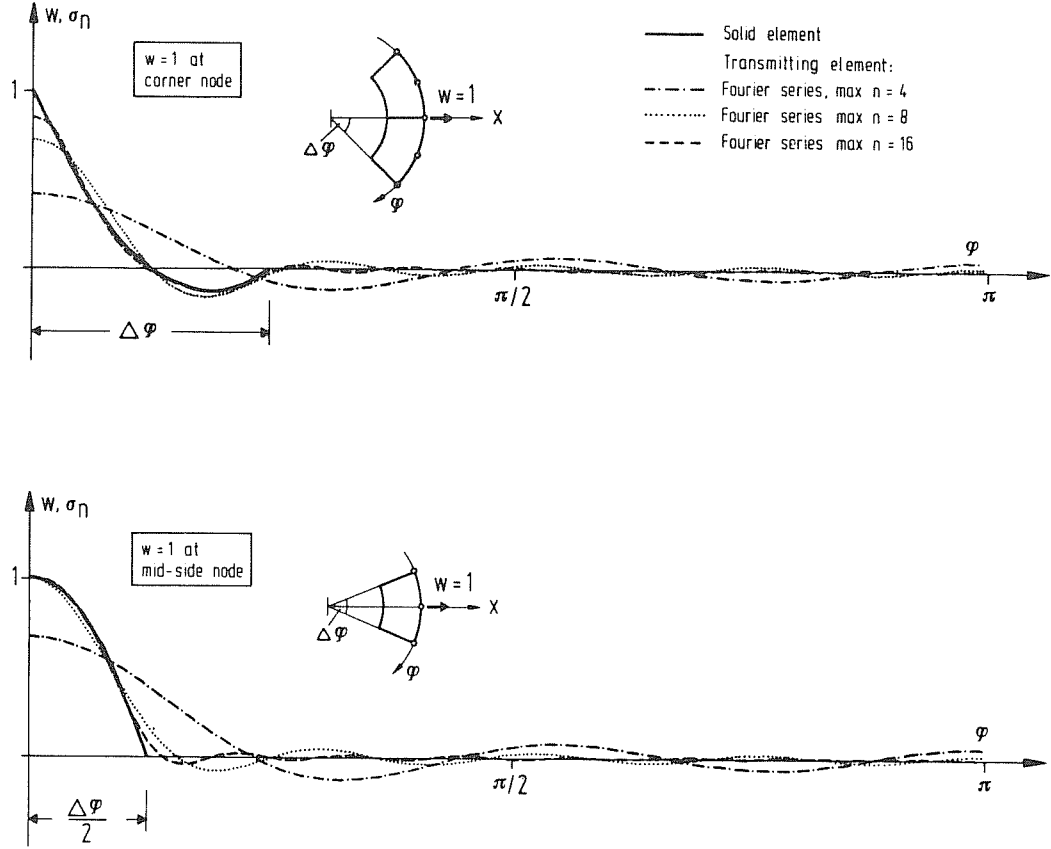


Figure 3. Approximation of a vertical unit nodal displacement by a Fourier series, element with  $\Delta\varphi = \pi/4$

is given in Figure 4 for  $\Delta\varphi = \pi/4, \pi/8, \pi/16$ . It may be concluded that the number of  $n = 2 \times \pi/\Delta\varphi$  is an appropriate choice. However, in practical analyses the variation of the displacements is generally much smoother than for a unit displacement at a single point. Hence in most cases considerably fewer Fourier coefficients are required for a suitable representation of the boundary displacement field.

### CYCLIC SYMMETRIC SYSTEMS

The analysis of cyclic symmetric systems can be significantly facilitated if only a section of the total system is considered. At the axes of symmetry the boundary conditions must take into account the symmetry of the displacement field. Moreover, the stiffness matrix of the transmitting element must be formulated for the reduced system. If  $m_p$  denotes the number of symmetry axes, the integration in equations (2a, b) is performed only in the range  $\varphi = 0$  to  $\varphi = 2\pi/m_p$ , resulting in the stiffness matrices  $A_{p,n}$  and  $S_{p,n}$  (instead of  $A_n$  and  $S_n$ ). The stiffness matrix of the reduced system is obtained for symmetric displacement fields as

$$\mathbf{R}^s = \frac{m_p}{\pi} \sum_{n_p} (1 - \frac{1}{2} \delta_{n0}) \mathbf{S}_{p,n}^T \mathbf{R}_n \mathbf{S}_{p,n} \quad (19a)$$

and for antisymmetric displacement fields as

$$\mathbf{R}^a = \frac{m_p}{\pi} \sum_{n_p} (1 - \frac{1}{2} \delta_{n0}) \mathbf{A}_{p,n}^T \mathbf{R}_n \mathbf{A}_{p,n} \quad (19b)$$



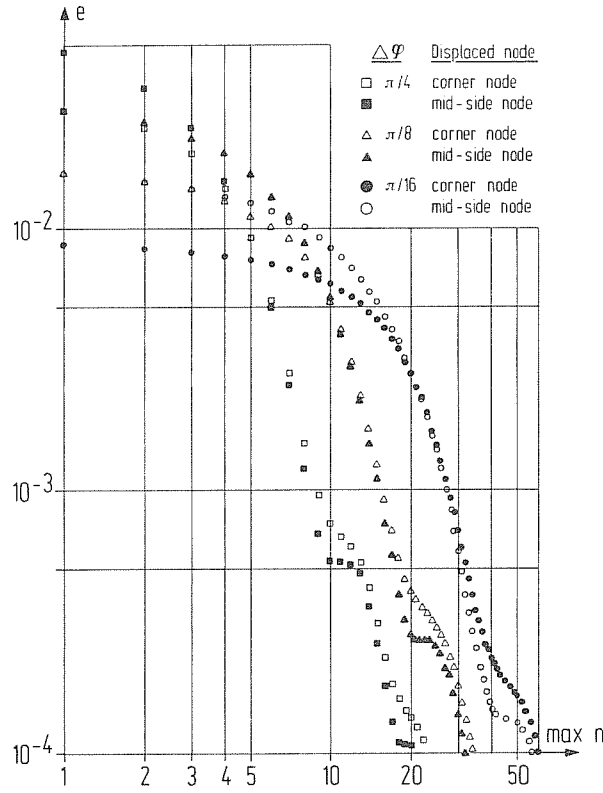


Figure 4. Mean square error of the displacements of the boundary

The summation has to be performed only for those Fourier modes  $n_p$  which have the same symmetry properties as the displacement field. Examples are given in Table II.

### EARTHQUAKE EXCITATION

The earthquake excitation of the soil model is defined as uniform motion of the rigid base. This corresponds to the assumption of vertically incident shear and compression waves. For cyclic symmetric displacements, the compression waves are described by

$$\mathbf{u}_n^s = \begin{Bmatrix} 0 \\ w_g + w_f \\ 0 \end{Bmatrix} \quad (20a)$$

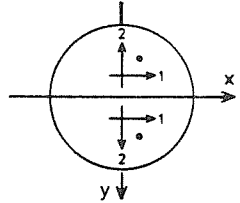
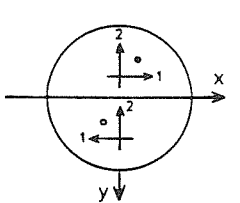
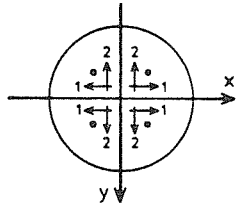
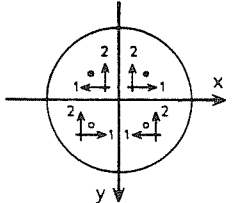
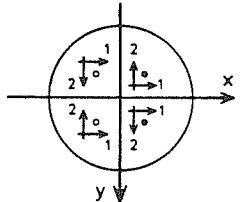
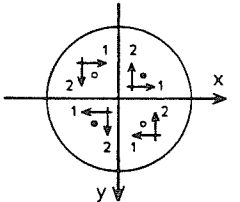
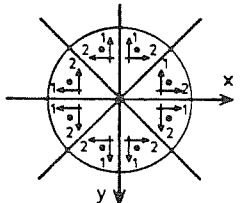
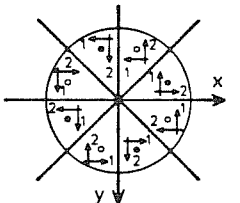
with  $n = 0$ , and the shear waves by

$$\mathbf{u}_n^s = \begin{Bmatrix} u_g + u_f \\ 0 \\ u_g + u_f \end{Bmatrix} \quad \text{or} \quad \mathbf{u}_n^a = \begin{Bmatrix} v_g + v_f \\ 0 \\ v_g + v_f \end{Bmatrix} \quad (20b, c)$$

with  $n = 1$ . The displacements  $u_g, v_g, w_g$  denote the motion of the rigid layer in the  $x$ -,  $y$ - and  $z$ -directions and  $u_f, v_f, w_f$  are the additional relative free field displacements. To determine the free field motion, again a piecewise linear or quadratic expansion in the vertical direction may be chosen.<sup>8</sup>

The earthquake excitation in the discretized domain results in a displacement of the rigid base as well as in

Table II. Fourier modes in symmetric systems with symmetric or antisymmetric displacement field

Displacement field		$m_p$	Fourier coefficient $n_p$
symmetric	antisymmetric		
		2	0, 1, 2, 3, 4, 5, . . . . .
		4	1, 3, 5, 7, 9, . . . . .
		4	0, 2, 4, 6, 8, . . . . .
		8	0, 4, 8, 12, 16, . . . . .

forces at the lateral boundary. The equations of motion of the element assembly can be written

$$(-\omega^2 \mathbf{M} + \mathbf{K} + \mathbf{R}^*) \mathbf{u}_{\text{rel}} = \omega^2 \mathbf{M} (\mathbf{e}_x u_g + \mathbf{e}_y v_g + \mathbf{e}_z w_g) + (\mathbf{R}^* - \mathbf{D}_u^*) \mathbf{u}_f^* + (\mathbf{R}^* - \mathbf{D}_v^*) \mathbf{v}_f^* + (\mathbf{R}^* - \mathbf{D}_w^*) \mathbf{w}_f^* \quad (21)$$

Here  $\mathbf{M}$  and  $\mathbf{K}$  are the mass and stiffness matrices of the discretized domain and  $\mathbf{u}_{\text{rel}}$  the relative nodal displacements;  $\omega$  denotes the circular frequency of the vibration. The vector  $\mathbf{e}_x$  contains ones in all degrees of freedom corresponding to a displacement in the  $x$ -direction and zeroes in all other degrees of freedom. Correspondingly  $\mathbf{e}_y$  and  $\mathbf{e}_z$  are defined for the  $y$ - and  $z$ -directions. The superscript '\*' indicates that the matrices and vectors defined initially for the nodal displacements at the boundary are augmented with zeroes so that they relate to all degrees of freedom of the discretized domain.

The expressions  $\mathbf{D}_u^* \mathbf{u}_f^*$ ,  $\mathbf{D}_v^* \mathbf{v}_f^*$  and  $\mathbf{D}_w^* \mathbf{w}_f^*$  describe those forces which are transferred in the free field (layered soil without structure in the discretized as well as in the infinite domain) between the regions  $r > r_0$  and  $r < r_0$ . For example, in the case of vertical excitation (compression waves) these forces are purely horizontal and are such that the radial displacements at the interface  $r = r_0$  are zero. The resulting cyclic symmetric forces

for  $n = 0$  (horizontal forces caused by compression waves) and  $n = 1$  (vertical forces caused by shear waves) are transformed into nodal forces. This leads to

$$\mathbf{D}_w = \frac{1}{2\pi} r_0 \mathbf{S}_0^T \mathbf{D}_0 \mathbf{S}_0 \quad (22a)$$

$$\mathbf{D}_u = \frac{1}{\pi} r_0 \mathbf{S}_1^T \mathbf{D}_1 \mathbf{S}_1 \quad (22b)$$

$$\mathbf{D}_v = \frac{1}{\pi} r_0 \mathbf{A}_1^T \mathbf{D}_1 \mathbf{A}_1 \quad (22c)$$

where  $\mathbf{D}_0$ ,  $\mathbf{D}_1$  are given in Reference 8 and  $\mathbf{S}_0$ ,  $\mathbf{S}_1$ ,  $\mathbf{A}_1$  are the transformation matrices  $\mathbf{S}_n$ ,  $\mathbf{A}_n$  for  $n = 0$  and  $n = 1$ , respectively.

The total displacements  $\mathbf{u}_{abs}$  in the discretized domain may be computed after the solution of equation (21) as

$$\mathbf{u}_{abs} = \mathbf{u}_{rel} + \mathbf{e}_x u_g + \mathbf{e}_y v_g + \mathbf{e}_z w_g \quad (23)$$

### EXAMPLE

The application of the method is demonstrated on a box-type structure embedded in a homogeneous soil layer, Figure 5. The structure has a Young's modulus of  $3 \times 10 \text{ kN/m}^2$ , a Poisson ratio of 0.2, a hysteretic damping ratio of 5 per cent and a mass density of  $2.5 \text{ t/m}^3$ . In the homogeneous layer the shear wave velocity is  $300 \text{ m/s}$ , the Poisson ratio 0.3, the hysteretic damping 5 per cent and the mass density  $1.8 \text{ t/m}^3$ . Two types of loading are considered. The structural response to a dynamic horizontal load acting at the top of the structure is studied in the frequency domain. Furthermore, the response of the system to an earthquake excitation is examined.

Due to the symmetry of the structure and the soil the finite element model can be reduced to a quarter of the

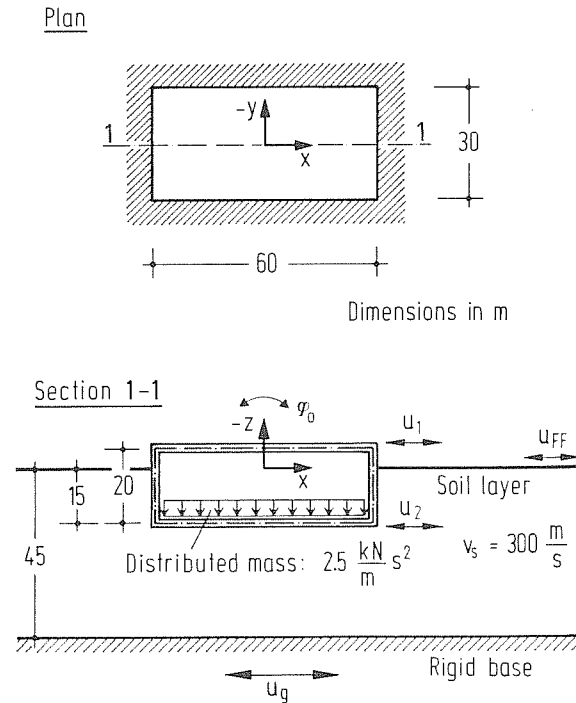


Figure 5. Embedded box-type structure

total system, Figure 6. The structure is modelled with combined plate and plane stress elements<sup>18</sup> and isoparametric solid elements with quadratic shape functions are used for the soil. When computing the stiffness matrix of the transmitting element the Fourier coefficients  $n = 1, 3, 5$  (see Table II) are used. The finite element model has 1066 degrees of freedom.

The transfer function of the horizontal and rocking motion at the top floor of the structure caused by a

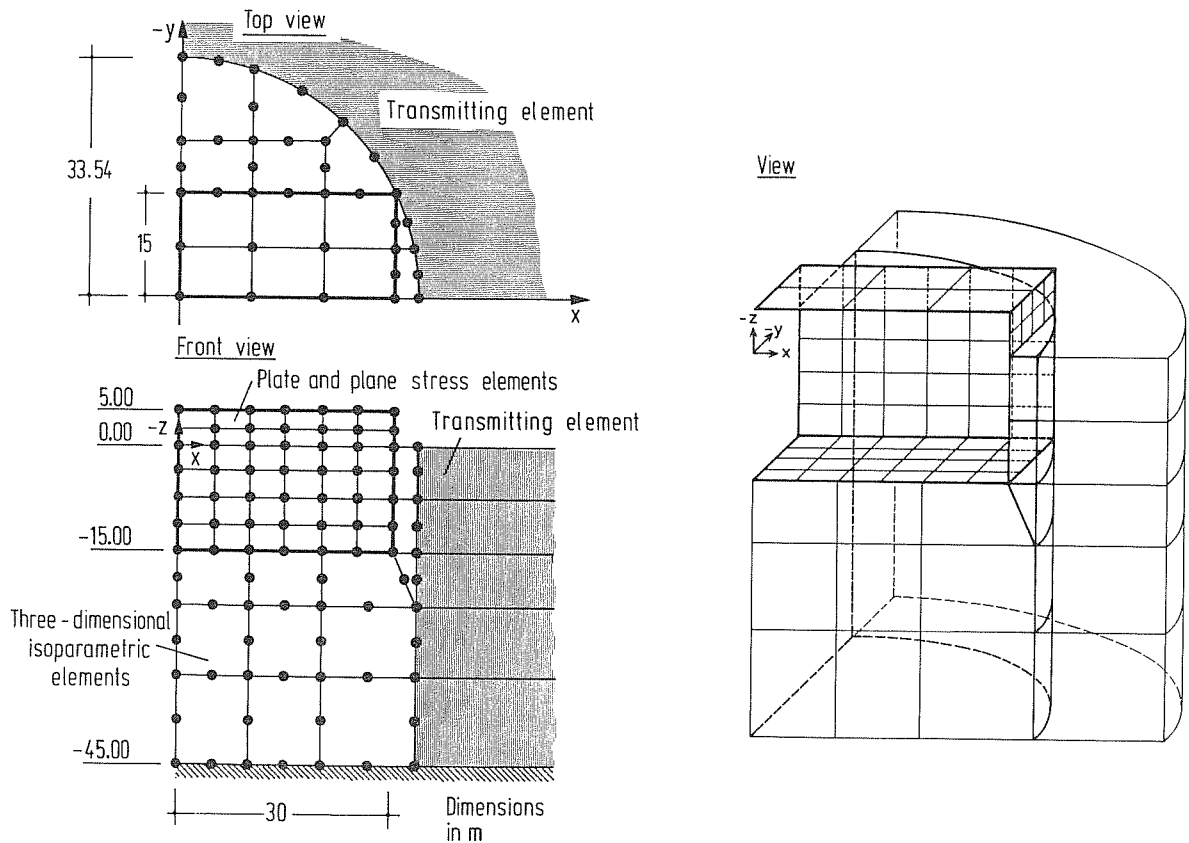


Figure 6. Finite element model

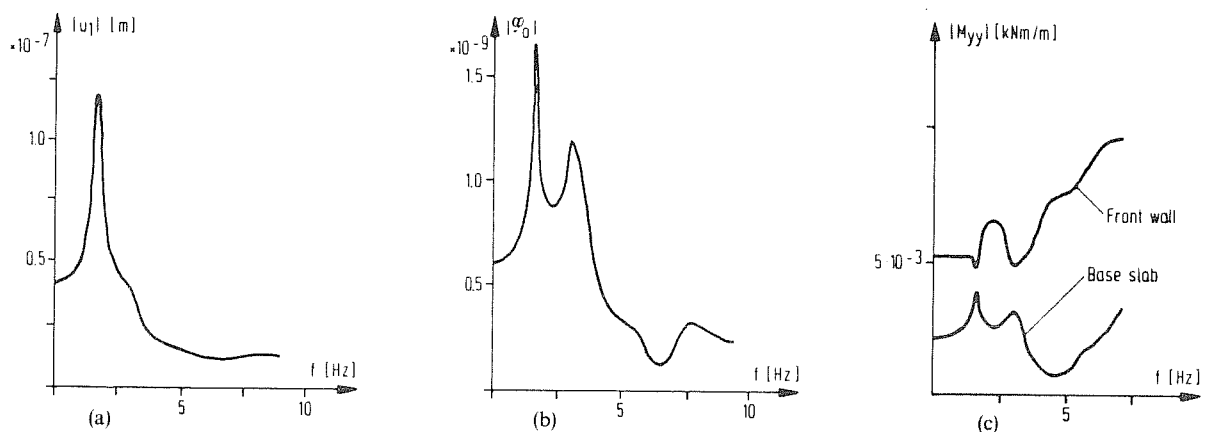


Figure 7. Transfer functions caused by a horizontal load  $P = 1$  kN: (a) horizontal displacement of the top slab; (b) rocking motion of the top slab; (c) bending moment in the base slab ( $x = 22.5$  m,  $y = 0$ ,  $z = 15$  m) and in the front wall ( $x = 30.0$  m,  $y = 0$ ,  $z = 5.6$  m)

horizontal load is shown in Figure 7. Peaks occur at the first natural frequencies of the layer for standing shear and compression waves, i.e. at 1.67 and 3.12 Hz, respectively. Figure 8 gives the structural displacements at different frequencies. At low frequencies the structure behaves essentially as a rigid body. However, the contribution of the structural deformations to the total displacements increases at higher frequencies, especially in the real part. The shear forces in the lateral wall  $y = 15$  m are transferred to the soil by the horizontal earth pressure and hence decrease with depth, Figure 9. The bending moments in the base slab are shown in Figure 10. Their distribution changes only slightly with the frequency and may be approximated by

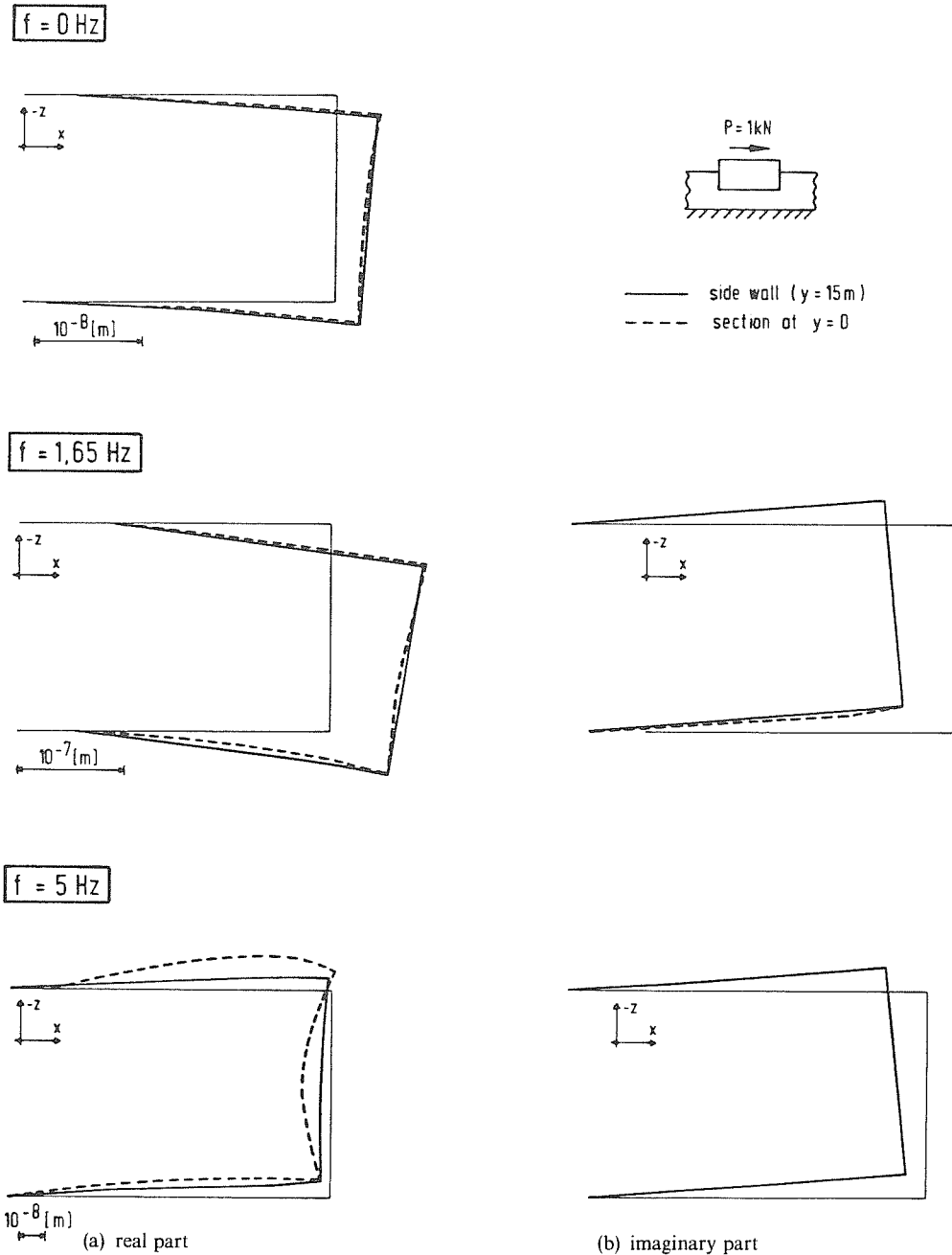
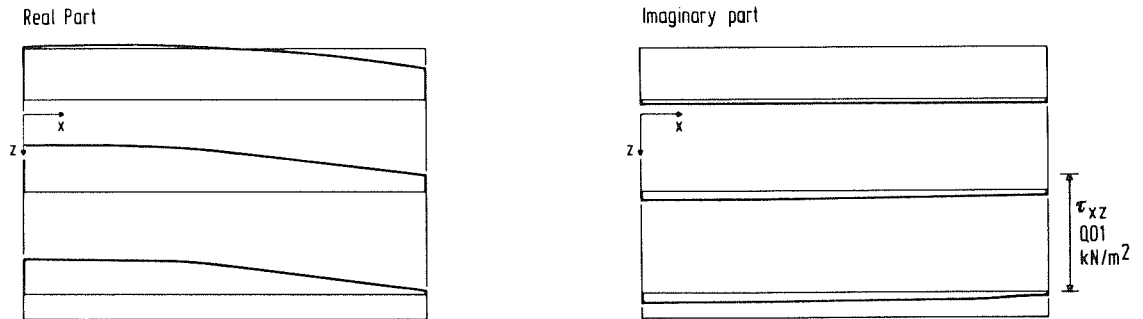


Figure 8. Displacements caused by a horizontal unit load ( $P = 1$  kN)

### Horizontal load



### Earthquake excitation $\ddot{u}_g = 1 \text{ m/s}^2$ $f = 1.65 \text{ Hz}$

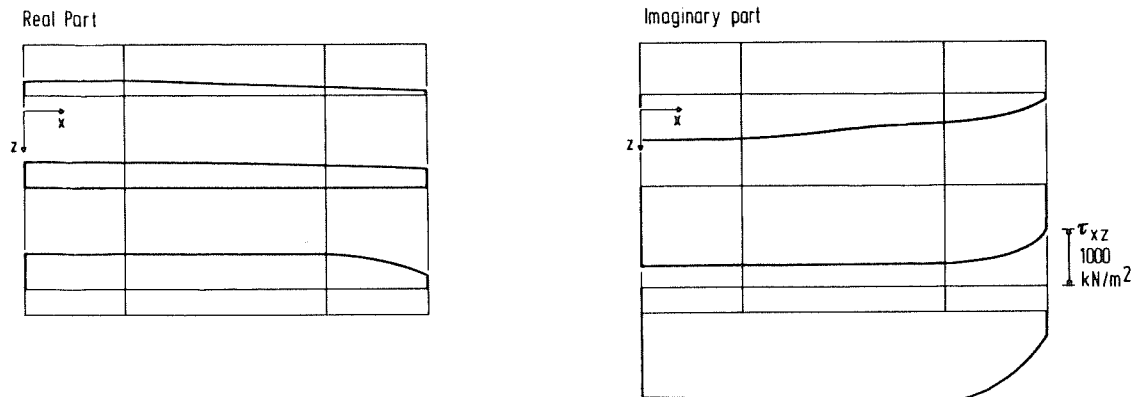
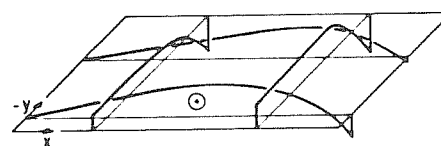
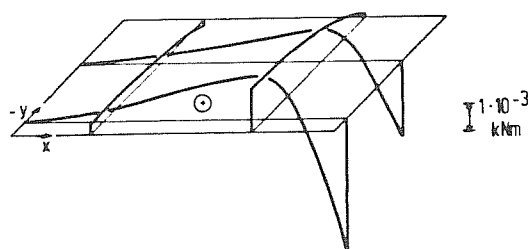


Figure 9. Shear stresses in the side wall ( $y = 15 \text{ m}$ )

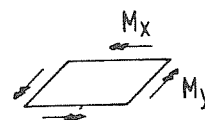
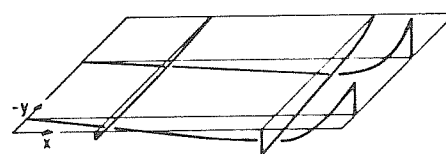
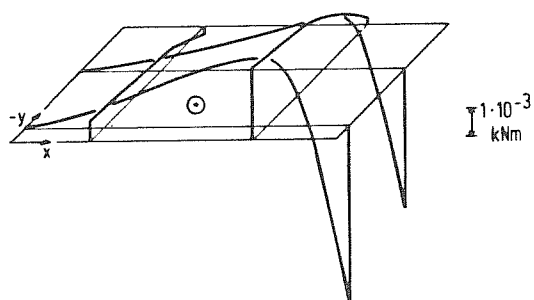
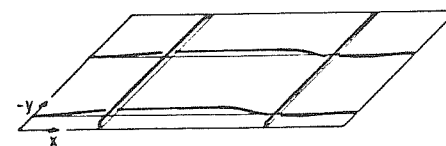
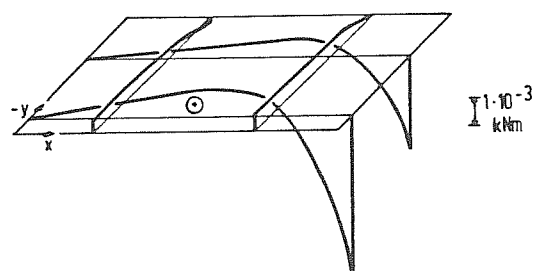
the static distribution. Their magnitude, however, varies considerably with frequency, Figure 7(c). The bending moment in the centre of the front wall, for example, equals the static value until the first natural frequency of the layer (1.67 Hz) and increases thereafter. This indicates an increase in the lateral dynamic earth pressure.

The earthquake response of the structure is studied for a horizontal motion of the rigid base. As the structure is light compared to the soil excavation it follows approximately the free field motion, Figures 11, 12. At higher frequencies some kinematic interaction effects, such as the rocking motion at  $f = 5 \text{ Hz}$ , occur. Also, the absolute value of the structural displacements related to the displacement at the free field surface decreases, Figure 13. The shear stresses in the side wall increase with depth, Figure 9. The distribution of the bending moments in the base slab and in the lateral wall  $x = 30 \text{ m}$  is typical for a pronounced swaying motion and changes only slightly with frequency, Figure 14, 15. The variation of their magnitude with frequency is similar to those of the structural displacements, Figure 11(c).

The structural accelerations were computed for a recorded time history, with the main frequencies between 1 and 5 Hz (Hollister Northern California on 9/3/1949, SO1W-component), defined at the free field surface. The maximum horizontal accelerations in the structure were computed to be  $0.80a_g$  at the top and  $0.74a_g$  at the base slab, where  $a_g$  is the maximum earthquake acceleration. This, as well as the time history of the response, indicates that the structure follows approximately the earthquake motion.

$f = 0$ 

(c)

 $f = 1,65 \text{ Hz}$  $f = 5,0 \text{ Hz}$ 

(a)

(b)

Figure 10. Bending moments in the base slab caused by a horizontal unit load ( $P = 1 \text{ kN}$ ): (a)  $M_{yy}$ —real part; (b)  $M_{yy}$ —imaginary part; (c)  $M_{xx}$ —real part

## CONCLUSIONS

A method for the finite element analysis of a non-axisymmetric soil model with an axisymmetric boundary has been presented. It is based on the transformation of a transmitting element with cyclic symmetric displacements to general displacement fields. The transformation has been applied to the semianalytical

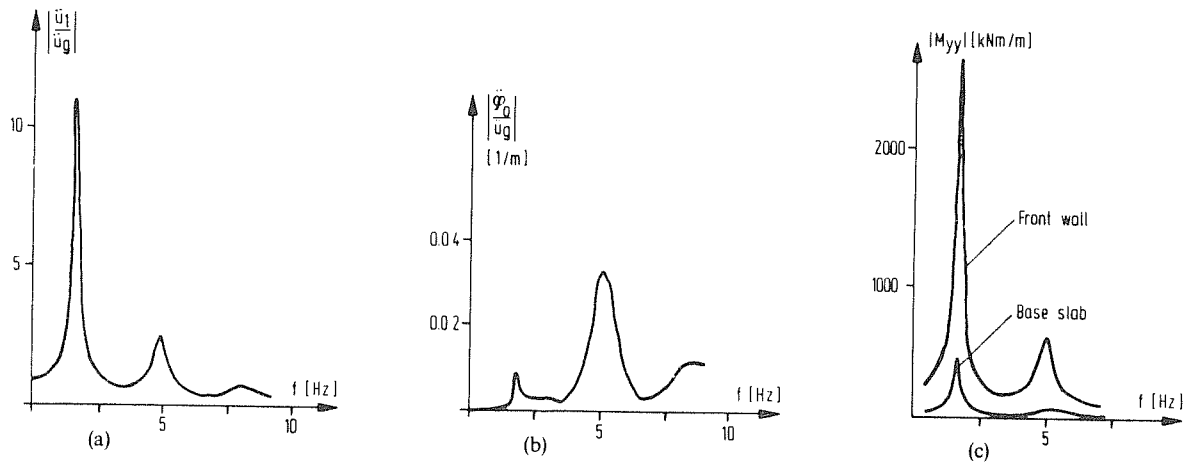


Figure 11. Transfer functions for horizontal earthquake excitation of the rigid base with  $\ddot{u} = 1 \text{ m/s}^2$ : (a) horizontal displacement of the top slab; (b) rocking motion of the top slab; (c) bending moment in the base slab ( $x = 22.5 \text{ m}$ ,  $y = 0$ ,  $z = 15 \text{ m}$ ) and in the front wall ( $x = 30.0 \text{ m}$ ,  $y = 0$ ,  $z = 5.6 \text{ m}$ )

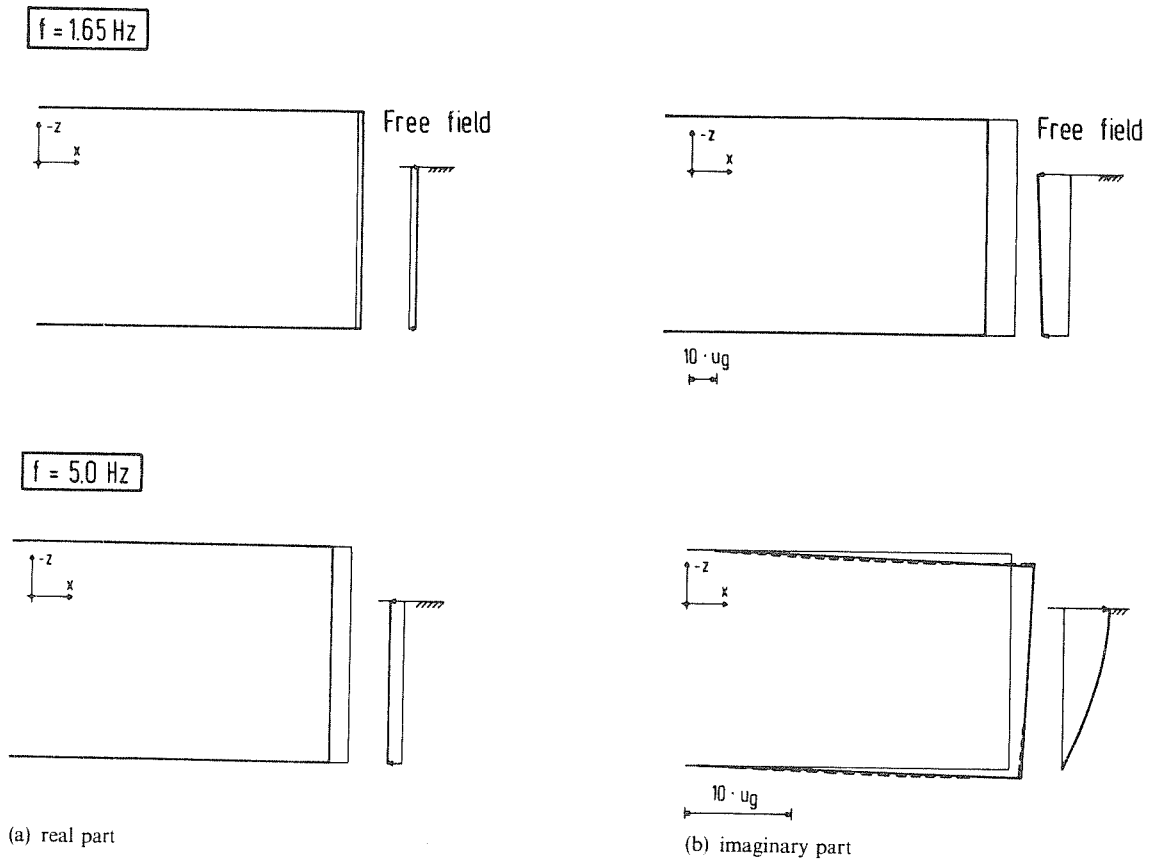
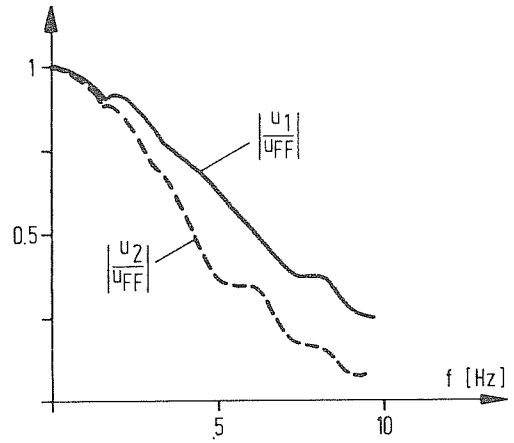


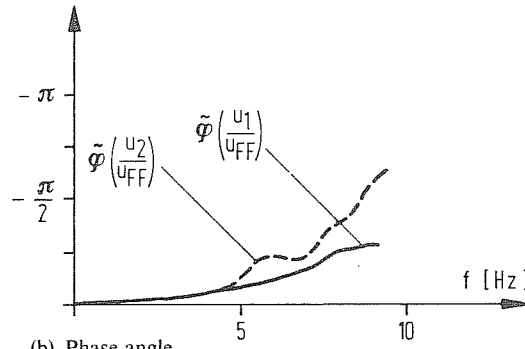
Figure 12. Displacements for horizontal earthquake excitation of the rigid base

element of Waas and Kausel.<sup>8,9</sup> However, other elements with cyclic symmetric displacement fields may also be used. This includes the application to the static and dynamic analysis of systems composed of axisymmetric and non-axisymmetric subsystems. The representation of the axisymmetric part of the structure by



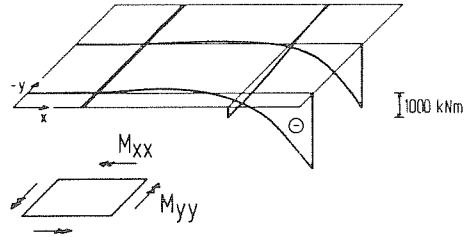
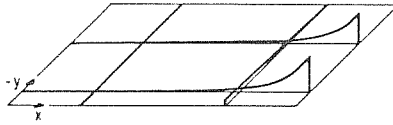
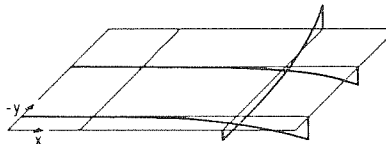
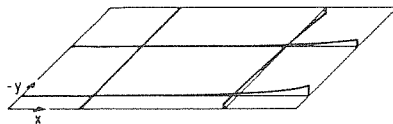


(a) Absolute value



(b) Phase angle

Figure 13. Transfer functions for horizontal earthquake excitation; horizontal structural motion, related to the motion at the surface of the free field

 $M_{yy}$  $M_{xx}$ 

(a) real part

(b) imaginary part

Figure 14. Bending moments in the base slab caused by a horizontal acceleration of the rigid base with  $\ddot{u} = 1 \text{ m/s}^2$  and  $f = 1.65 \text{ Hz}$

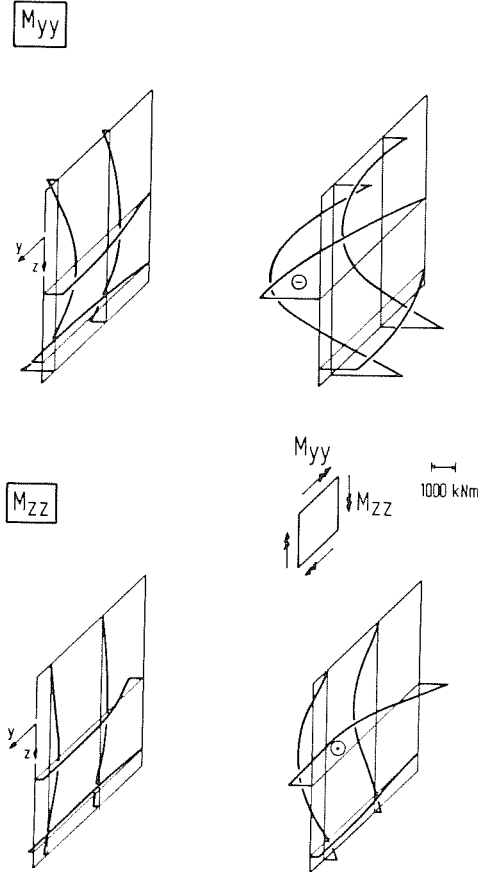


Figure 15. Bending moments in the front wall ( $x = 30$  m) caused by a horizontal acceleration of the rigid base with  $\ddot{u} = 1 \text{ m/s}^2$  and  $f = 1.65 \text{ Hz}$

axisymmetric elements can reduce considerably the numerical effort as compared to a full three-dimensional analysis of the entire system.

The method is illustrated by the dynamic analysis of an embedded building. The global accelerations agree well with those obtained by a simple beam model with appropriately calculated frequency-dependent springs and dampers to model the soil.<sup>19</sup> The finite element model, however, enables a considerably more detailed determination of the section forces in the structure. The results indicate the important effects of the lateral dynamic earth pressure on the magnitude and the distribution of the section forces in the base walls.

#### APPENDIX: COMPUTATION OF THE TRANSFORMATION MATRICES

In equations (11c, d) the following integrals are to be calculated:

$$\int \Phi_n^s \mathbf{T} d\varphi = \begin{bmatrix} I_7 & I_{13} & 0 \\ 0 & 0 & I_1 \\ I_{16} & -I_{10} & 0 \end{bmatrix} \quad (\text{A1})$$

$$\int \Phi_n^s \mathbf{T} \varphi d\varphi = \begin{bmatrix} I_8 & I_{14} & 0 \\ 0 & 0 & I_2 \\ I_{17} & -I_{11} & 0 \end{bmatrix} \quad (\text{A2})$$

$$\int \Phi_n^s \mathbf{T} \varphi^2 d\varphi = \begin{bmatrix} I_9 & I_{15} & 0 \\ 0 & 0 & I_3 \\ I_{18} & -I_{12} & 0 \end{bmatrix} \quad (\text{A3})$$

$$\int \Phi_n^a \mathbf{T} d\varphi = \begin{bmatrix} I_{10} & I_{16} & 0 \\ 0 & 0 & I_4 \\ -I_{13} & I_7 & 0 \end{bmatrix} \quad (\text{A4})$$

$$\int \Phi_n^a \mathbf{T} \varphi d\varphi = \begin{bmatrix} I_{11} & I_{17} & 0 \\ 0 & 0 & I_5 \\ -I_{14} & I_8 & 0 \end{bmatrix} \quad (\text{A5})$$

$$\int \Phi_n^a \mathbf{T} \varphi^2 d\varphi = \begin{bmatrix} I_{12} & I_{18} & 0 \\ 0 & 0 & I_6 \\ -I_{15} & I_9 & 0 \end{bmatrix} \quad (\text{A6})$$

The integrals  $I_1$ – $I_{18}$  are defined as follows and can be expressed by the integrals H1(n)–H6(n), given as a function of  $n$ :

$$\begin{aligned} I_1 &= \int \cos n\varphi d\varphi &= \text{H1}(n) \\ I_2 &= \int \varphi \cos n\varphi d\varphi &= \text{H2}(n) \\ I_3 &= \int \varphi^2 \cos n\varphi d\varphi &= \text{H3}(n) \\ I_4 &= \int \sin n\varphi d\varphi &= \text{H4}(n) \\ I_5 &= \int \varphi \sin n\varphi d\varphi &= \text{H5}(n) \\ I_6 &= \int \varphi^2 \sin n\varphi d\varphi &= \text{H6}(n) \\ I_7 &= \int \cos \varphi \cos n\varphi d\varphi &= \frac{1}{2} \text{H1}(1-n) + \frac{1}{2} \text{H1}(1+n) \\ I_8 &= \int \varphi \cos \varphi \cos n\varphi d\varphi &= \frac{1}{2} \text{H2}(1-n) + \frac{1}{2} \text{H2}(1+n) \\ I_9 &= \int \varphi^2 \cos \varphi \cos n\varphi d\varphi &= \frac{1}{2} \text{H3}(1-n) + \frac{1}{2} \text{H3}(1+n) \\ I_{10} &= \int \cos \varphi \sin n\varphi d\varphi &= \frac{1}{2} \text{H4}(n-1) + \frac{1}{2} \text{H4}(n+1) \\ I_{11} &= \int \varphi \cos \varphi \sin n\varphi d\varphi &= \frac{1}{2} \text{H5}(n-1) + \frac{1}{2} \text{H5}(n+1) \\ I_{12} &= \int \varphi^2 \cos \varphi \sin n\varphi d\varphi &= \frac{1}{2} \text{H6}(n-1) + \frac{1}{2} \text{H6}(n+1) \\ I_{13} &= \int \sin \varphi \cos n\varphi d\varphi &= \frac{1}{2} \text{H4}(1-n) + \frac{1}{2} \text{H4}(1+n) \end{aligned}$$

$$I_{14} = \int \varphi \sin \varphi \cos n\varphi \, d\varphi = \frac{1}{2} H5(1-n) + \frac{1}{2} H5(1+n)$$

$$I_{15} = \int \varphi^2 \sin \varphi \cos n\varphi \, d\varphi = \frac{1}{2} H6(1-n) + \frac{1}{2} H6(1+n)$$

$$I_{16} = \int \sin \varphi \sin n\varphi \, d\varphi = \frac{1}{2} H1(1-n) - \frac{1}{2} H1(1+n)$$

$$I_{17} = \int \varphi \sin \varphi \sin n\varphi \, d\varphi = \frac{1}{2} H2(1-n) - \frac{1}{2} H2(1+n)$$

$$I_{18} = \int \varphi^2 \sin \varphi \sin n\varphi \, d\varphi = \frac{1}{2} H3(1-n) - \frac{1}{2} H3(1+n)$$

The analytical solution of the integrals H1(n)–H6(n) is elementary.

#### REFERENCES

1. J. Lysmer, 'Analytical procedures in soil dynamics', State of the art, *Proc. ASCE geotech. eng. div. specialty conf. earthquake eng. soil dyn.* Pasadena, California III (1978).
2. G. Waas, 'Berechnung dynamischer Boden-Bauwerk-Wechselwirkungen', *Proc. 'Finite Elemente—Anwendung in der Bautechnik'*, München, Germany (1984), Wilhelm Ernst & Sohn, Berlin, 1985.
3. J. Lysmer and R. L. Kuhlemeyer, 'Finite dynamic model for infinite media', *J. eng. mech. div. ASCE*, **95**, 859–877 (1969).
4. J. M. Roesset and M. M. Ettouney, 'Transmitting boundaries: a comparison', *Int. j. numer. anal. methods geomech.* **1**, 151–176 (1977).
5. W. Haupt, 'Dynamic analysis of three-dimensional soil models by a finite element method', *Proc. dyn. methods soil rock mech.* Karlsruhe I (1977), Balkema, Rotterdam, 1978.
6. S. Gupta, J. Penzien, T. W. Lin and C. S. Yeh, 'Three-dimensional hybrid modelling of soil–structure interaction', *Earthquake eng. struct. dyn.* **10**, 69–87 (1982).
7. G. Waas, 'Linear two-dimensional analysis of soil dynamics problems in semi-infinite media', *Dissertation*, University of California, Berkeley, 1972.
8. E. Kausel, 'Forced vibrations of circular foundations on layered media', *MIT Research Report R74-11*, MIT, Cambridge, Mass., 1974.
9. E. Kausel, J. M. Roesset and G. Waas, 'Dynamic analysis of footings on layered media', *J. eng. mech. div. ASCE* **101**, 679–693 (1975).
10. J. Lysmer, T. Udaka, C.-F. Tsai and H. B. Seed, 'Flush—a computer program for approximate 3-d-analysis of soil–structure interaction problems', *Report No. EERC 35-30*, Earthquake Engineering Research Center, University of California, Berkeley, CA, 1975.
11. A. Gomez-Masso, J. Lysmer, J. Chen and B. Seed, 'Soil–structure interaction with Rayleigh waves', *Earthquake eng. struct. dyn.* **11**, 567–583 (1983).
12. G. Waas and W. Weber, 'Soil structure interaction analysis by different methods', *SMIRT 5*, Berlin (1979).
13. K. Sezawa, 'Further studies on Rayleigh waves having some azimuthal distribution', *Bull. earthquake res. inst. Tokyo Univ.* **6**, 1–18 (1929).
14. G. Waas, H. R. Riggs and H. Werkle, 'Displacement solutions for dynamic loads in a transversely-isotropic stratified medium', *Earthquake eng. struct. dyn.* **13**, 173–193 (1985).
15. O. C. Zienkiewicz, *The Finite Element Method in Engineering Science*, 2nd edn, McGraw-Hill, London, 1971.
16. K. E. Buck, 'Rotationskoerper unter beliebiger Belastung', in *Finite Elemente in der Statik*, Wilhelm Ernst & Sohn, Berlin, 1973.
17. H. Werkle, 'Ein Randelement zur dynamischen Finite-Element-Berechnung dreidimensionaler Baugrundmodelle', *Dissertation*, Universität Karlsruhe, Germany, 1981.
18. R. W. Clough and C. A. Felippa, 'A refined quadrilateral element for analysis of plate bending', *Proc. 2nd conf. matrix methods struct. mech.* Wright Patterson AFB, Ohio (1968).
19. F. P. Müller and H. Werkle, 'Dynamic analysis of three-dimensional soil models by a finite element method', *SMIRT 6*, Paris (1981).